EJNMMI Physics

ORIGINAL RESEARCH Open Access

A critical phantom study of the energy window used for ^{99m}Tc quantitative explorations with a ring CZT SPECT system

Alain Seret[1*] and Claire Bernard[2]

*Correspondence:
aseret@uliege.be

[1] GIGA Institute, University of Liège, Institut de Physique B5a, Allée du six Août, 19, 4000 Liège, Belgium
[2] CHU Liège, Service de Radiophysique Médicale, Médecine nucléaire et imagerie oncologique, Avenue de l'Hôpital, 1, 4000 Liège, Belgium

Abstract

Background: This study investigated, mainly for quantitative ^{99m}Tc explorations with a ring CZT SPECT system (GE HealthCare Starguide), the use of a narrow symmetric or a fully asymmetric energy window to reject scattered photons. The results were compared with the manufacturer's post-acquisition dual energy window approach.

Methods: Two uniform and two cold and hot rod contrast cylindrical phantoms of various sizes were scanned with the Starguide system to acquire a very high number of counts. After rebinning the list-mode files for different energy windows, data were reconstructed with manufacturer's iterative algorithm including attenuation correction, resolution recovery and eventually scatter correction, but without any regularization technique. Cold rod residual scatter fraction, hot and cold rod contrast recovery coefficient, coefficient of variation in phantom uniform areas and quantification accuracy using calibration with one of the homogeneous phantoms were, among others, computed.

Results: Narrow symmetric photopeak-centred windows or fully asymmetric (≥ 140 keV) window led, on one hand, to decreased scatter residual fraction and sensitivity and, on the other hand, to increased noise, cold and hot recovery coefficients when compared to a standard 15–20% wide symmetric window. With a 6–7% wide symmetric window we obtained very comparable results to the dual energy window scatter correction used by the manufacturer for all measured parameters, but larger recovery coefficients especially for small hot objects in a cold background. Similar results were obtained with the fully asymmetric window at the cost of a higher noise level resulting from a drastic reduction of the sensitivity.

Conclusions: Narrow symmetric or asymmetric energy windows were found an interesting alternative to the standard dual energy window method to reject ^{99m}Tc scattered photons. As a key feature, they allowed to avoid the erasing of small hot objects in a null background that was observed with the standard dual energy window scatter correction.

Keywords: CZT, Energy window, Scatter, SPECT

Background

Cadmium zinc telluride (CZT)-based detectors offer better energy resolution than the standard NaI scintillation detectors [1–4]. Nevertheless, manufacturers of SPECT systems equipped with this new detector generation still recommend 15–20% wide energy windows [4, 5]. In their early software versions, they also used energy window-based scatter correction (SC) methods, namely dual (DEW) or triple (TEW) energy windows, that were validated for use with NaI systems [6–8]. However, the spectrum structures of the scattered photons are not similar for NaI and CZT [2, 9]. Therefore, a simple transposition of the spectrum-based scatter correction techniques developed for NaI detectors to the new CZT systems is highly questionable [9].

Very recently, we extended our past comparative survey for quantitative ^{99m}Tc imaging of SPECT-CT [10] to the three large field-of-view CZT-based SPECT systems available on the market [11]. The results seriously questioned the wide energy windows advocated by the manufacturers and even more so their scatter correction strategies, at least as they were at the time of the study. This was dramatically highlighted for the Starguide CZT ring systems by the absence, in the scatter corrected image, of the thinnest hot rods in a null background of our custom phantom [10, 11], whereas they were well contrasted in the non-scatter corrected images [11].

For the Starguide system, the access to the list-mode rebinning software is free for any user. In the present study, Starguide data acquired in our previously mentioned comparative study [11] were reprocessed using the system's list-mode rebinning software to investigate the effects of narrower or asymmetric energy windows on scatter residual fraction, hot and cold contrast recovery coefficients, and quantification accuracy.

Methods

Phantoms

Three different cylinders were used to obtain four different phantoms (Table 1) [10, 11]. One phantom (NEMA) corresponded to the NEMA NU2-1994 attenuation and scatter correction accuracy phantom with its three air, water and Teflon inserts [12]. The second cylinder was used with custom cold and hot rod inserts (TOM) for contrast recovery evaluation (Figs. 1, 2) and filled with water without any object inside (XL) for calibration purposes. The third phantom (L) was a water-filled cylinder devoid of any other object,

Table 1 Physical characteristics of the phantoms

Name	Diameter (mm)	Height (mm)	Inserts			Water volume (ml)
			Type	Diameter (mm)	Offset from cylinder axis (mm)	
L	94	80	None			570
NEMA	200	190	Air Water, Teflon rods	30	60	4245
TOM	200	300	Plastic rods*	25	0	6025
				6,8,10,12,16,20	50	
			Water rods* in plastic	20	0	
				4,6,8,10,13,16	50	
XL	200	300	None			9940

* 85 mm tall

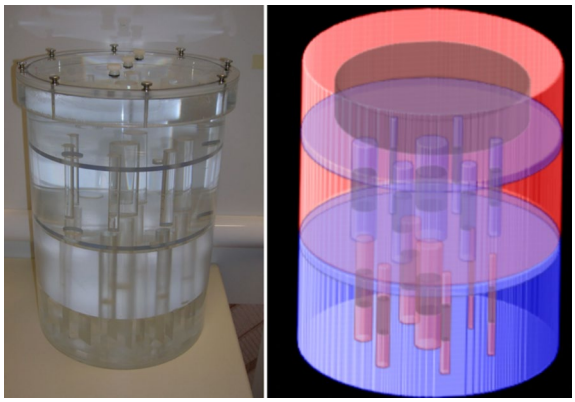

Fig. 1 Structure of TOM phantom. Left: photography. Right: 3D sketch of the three phantom parts used in this work: uniform compartment (top), cold (middle) and hot (bottom) rod inserts. Cold areas are in blue, hot areas in red and the processing ROIs (uniform and ROIF in rods) in brownish. The holes in the plate which allow a free circulation of the liquid between all compartments are not represented on the sketch but are well visible on the photography. Reproduced from [11]

used as cross-check of the calibration factors when using phantoms of very different volumes (factor of 17 between L and XL). In TOM phantom (Figs. 1, 2), the largest cold and hot rods were located on the cylinder main axis whereas the other rods were equally angularly spaced with their centre at a distance of 50 mm from this axis. TOM also contained a 40 mm thick grid with square plastic elements of 22 mm side-spaced by 12 mm that was not further considered in this study. The three inserts of TOM left a uniform space of 65 mm height, and water could freely move across all parts, allowing to get an identical activity concentration in all hot areas of the phantom.

At start of acquisition, the activity was 330 MBq in L, 696 MBq in NEMA, 582 MBq in TOM and 789 MBq in XL. This corresponded within 10% to our standardized conditions (300 MBq in L and 740 MBq in the three large phantoms [10, 11]), excepting in TOM where the activity was 22% lower due to a delayed acquisition start. Thorough shaking of the phantoms allowed to obtain a uniform distribution of activity in all hot compartments. The injected activities were carefully measured with the radionuclide calibrator (IBC Lite, Veenstra, Joure, The Netherlands) available in the department, and the time of measurement was recorded. This radionuclide calibrator undergoes daily and periodic quality controls as requested by the Belgian Federal Agency for Nuclear Control. In a national survey, these procedures have been shown to allow 5% accuracy for ^{99m}Tc measurements [13].

Data acquisition

The data of this study were recorded in list-mode with the ring CZT-based SPECT-CT Starguide (GE HealthCare, Haifa, Israel) fitted with its standard collimator and using the manufacturer standard acquisition software (version 1.003.407.0). Each phantom was scanned once. As TOM and XL were a little longer than the SPECT field of view, their upper part where screws are located was skipped. It was ensured that the scan procedure focussed as much as possible on the phantom. The heads positioning was guided by the built-in optical system. The focus mode [14] was enabled, with the focus percentage set to 100%. The number of rotations was left as automatically selected by the system. There

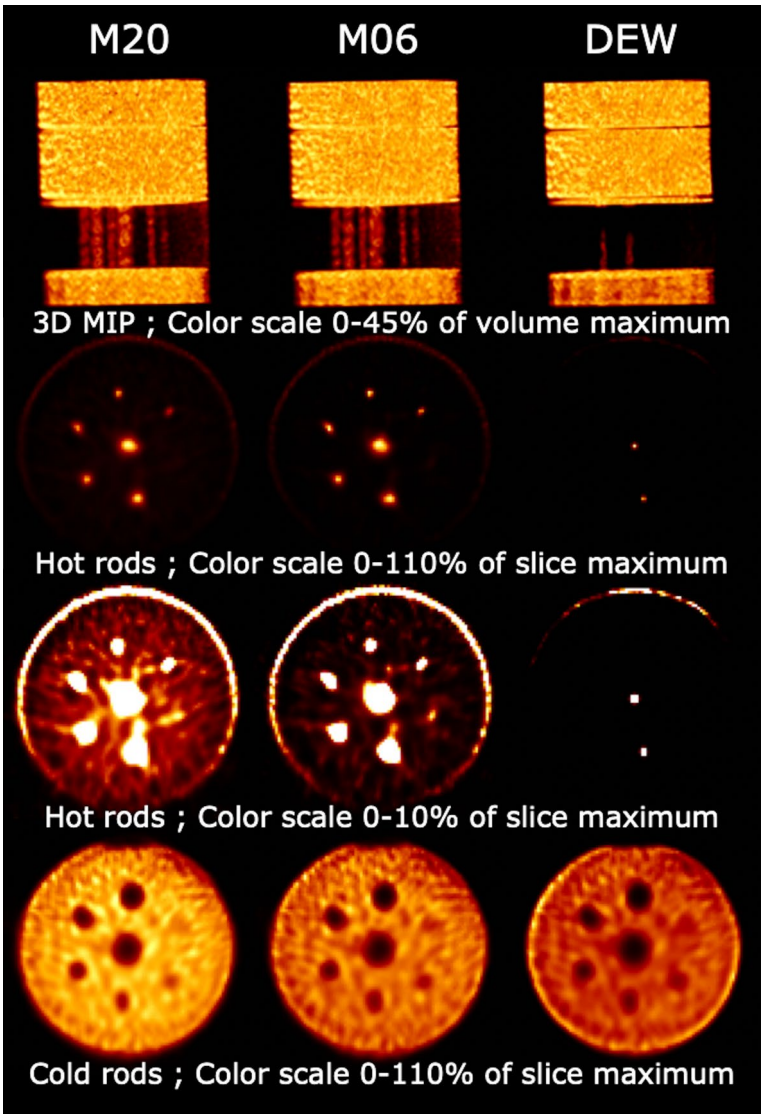

Fig. 2. 3D maximum intensity rendering (row 1), 30-mm thick transverse slice of the hot (rows 2–3) and cold (row 4) rod parts of TOM phantom for M20img (left), M06img (centre) and DEWimg (right)

were 6 rotations for the three large phantoms and 4 for the smaller L phantom. The heads sweep mode was continuous and the sweep step 2°. The pixel size was 2.46 mm. A standard low dose CT scan was also performed and used for attenuation correction.

List-mode data were rebinned in projections for six different main energy windows. Five were symmetric photopeak-centred (140 keV) and 20 (M20), 15 (M15), 10 (M10), 7 (M07) and 6 (M06) % wide, the sixth was fully asymmetric and 10% wide (MA), extending therefore from 140 to 154 keV. The first two widths were chosen because they are commonly used with NaI-based SPECT systems but also because of the manufacturer's recommended widths. Rebinning was also performed for the 114–126 keV window (S10) used by the manufacturer as secondary window for scatter correction with DEW. The rebinning acquisition time used for all windows was the time necessary to get our standardized [10, 11] total number of counts with NEMA, TOM and XL (100 Mcounts),

and L (85 Mcounts) for the M20 rebinned projections. These times were 25 min for L, 35 min for NEMA and XL, 45 min for TOM. The real scan durations were a few minutes longer. This strategy of identical acquisition time for all energy windows allowed us to directly compare and quantify, for each phantom, the counts loss and the noise increase in the final reconstructed images due to the change of the energy window. Following GE Healthcare, no specific uniformity correction was required either for the symmetric windows or the asymmetric window.

Reconstruction

The seven sets of rebinned projections were reconstructed with the manufacturer's standard OSEM algorithm (software version 1.0.10.0), CT-based attenuation correction and resolution recovery for a total of 200 updates (10 subsets and 20 iterations). We previously observed that convergence was almost reached for this number of updates [11]. An additional set of images was also obtained using DEW scatter correction as implemented by the manufacturer. In particular, the weighting factor of the secondary window was not modifiable and the manufacturer's default value was used. Eight sets of images were therefore available per phantom, seven without software scatter correction: M20img, M15img, M10img, M07img, M06img, MAimg and S10img; the eighth, DEWimg, was reconstructed with the manufacturer's DEW scatter correction strategy. No pre-filter, post-filter, nor any noise reduction techniques were applied as in our previous studies [10, 11].

Image processing

Parameters

The reported parameters were obtained by drawing regions of interest (ROI), on the reconstructed images, in the rods and in the uniform part of the phantoms using the methods described in detail elsewhere [10, 11]. These ROIs were drawn on the nuclear medicine images but their positioning was checked on the CT images and eventually corrected. The mean number of counts (MNC) per pixel was obtained in each ROI. For the ROIs drawn in the uniform parts, the standard deviation ($SD_{Uniform}$) was also determined.

The residual fraction (RF) in the cold inserts of the NEMA phantom was defined as the ratio of MNC in cold insert ROI (MNC_{Rod}) and average MNC in eight ROIs drawn in the background ($MNC_{Background}$) following NEMA NU2-1994 procedure [12]:

$$RF = \frac{MNC_{Rod}}{MNC_{Background}}$$

The recovery coefficients (RC) in the rods of the contrast phantom TOM were computed from cylindrical regions of interest of full (ROIF) (Fig. 1) and half (ROIH) rod physical diameter and a large ROI in the uniform part of TOM. The ROIs were centred in the rods and 30-mm tall. The ROI in the uniform part was a cylinder of 160-mm diameter and 24-mm height. The recovery coefficient in cold rods (RCcold) was one minus the ratio of MNCs between the rod ROI (MNC_{ROI}) and the uniform part ROI ($MNC_{Uniform}$):

$$RC_{cold} = 1 - \frac{MNC_{ROI}}{MNC_{Uniform}}$$

The recovery coefficient in hot rods (RChot) was the ratio of MNCs between the rod ROI and the uniform part ROI:

$$RC_{hot} = \frac{MNC_{ROI}}{MNC_{Uniform}}$$

The free circulation of the radioactive liquid between all compartments of TOM allowed the use of this very simple parameter which did not need activity measurements.

From $SD_{Uniform}$ and $MNC_{Uniform}$, the coefficient of variation (COV) was computed and used as a metric for reconstructed noise in a large uniform area of each phantom:

$$COV = \frac{SD_{Uniform}}{MNC_{Uniform}}$$

RF, RCcold, RChot, and COV were expressed in percent.

MNC in the phantom uniform part for the different energy window settings and for the DEW corrected image sets were compared using the R20 parameter, defined as the ratio between MNC in a specific window (MNC_{Window}) or with DEW (MNC_{DEW}) and in $M20_{img}$ (MNC_{M20}):

$$R20 = \frac{MNC_{WindoworDEW}}{MNC_{M20}}$$

M20 was taken as the reference because it is the main window used by the manufacturer in DEW scatter correction, as previously mentioned.

Post reconstruction DEW corrected results

We also generated a set of RF and RC values, called PostReconDEW as they were computed from the M20img and S10img, as follows. The DEW technique allows the computation of scatter corrected MNC (MNC_{SC}) from MNC_{M20} and S10img MNC (MNC_{S10}) using the equation [6]:

$$MNC_{SC} = MNC_{M20} - k * MNC_{S10}$$

where k is a constant that is to be experimentally determined. In this study, we decided to use the k value which should lead to the same count subtraction than the manufacturer's implementation of DEW. To this end, the above equation was first applied to the MNC values in the uniform parts of the four phantoms. It was found to be $k = 1.10 \pm 0.01$. The above equation with this $k = 1.1$ was then applied to the MNC of ROIs drawn in the inserts of NEMA and TOM. Finally, PostReconDEW RF in NEMA and RC in TOM were computed as described above.

Quantification accuracy

Several large ROIs of different sizes were also drawn in L and XL images as the ROI size used for calibration with a uniform phantom is a subject of debate [15, 16]. The height and diameter of these regions were equal (ROI0) to the phantom physical diameter and

height, 2 cm or 4 cm smaller (ROI − 2, ROI − 4) or larger (ROI + 2, ROI + 4). ROI − 4 was too small and discarded for L. An additional ROI encompassing the whole reconstructed image (ROIimg) was also considered. From MNC in these ROIs, the ROIs volume and the decay corrected activity concentration [17], conversion factors (CF), also sometimes called calibration factors, were computed for both L and XL phantoms and each ROI [10, 11]. The volume of any ROI larger than the phantom physical sizes was renormalized to ROI0 volume. CF allowed to convert MNC in a ROI drawn in another phantom into activity concentration (Ames). CF from both L and XL were applied to MNC in the hot area of NEMA to obtain Ames in this phantom [10, 11]. Moreover, CF obtained from XL were also applied to the smaller L phantom in order to check the impact of phantom size on the quantification accuracy. The quantification error (QE) is the relative deviation from the true activity concentration (Atrue):

$$QE = \frac{A_{mes}}{A_{true}} - 1$$

QE was expressed in percent.

Results

The images obtained with the largest and narrowest symmetric energy windows are illustrated in Fig. 2 together with the images obtained with the manufacturer implementation of DEW for scatter correction. Figure 3 illustrates the variations of R20 and

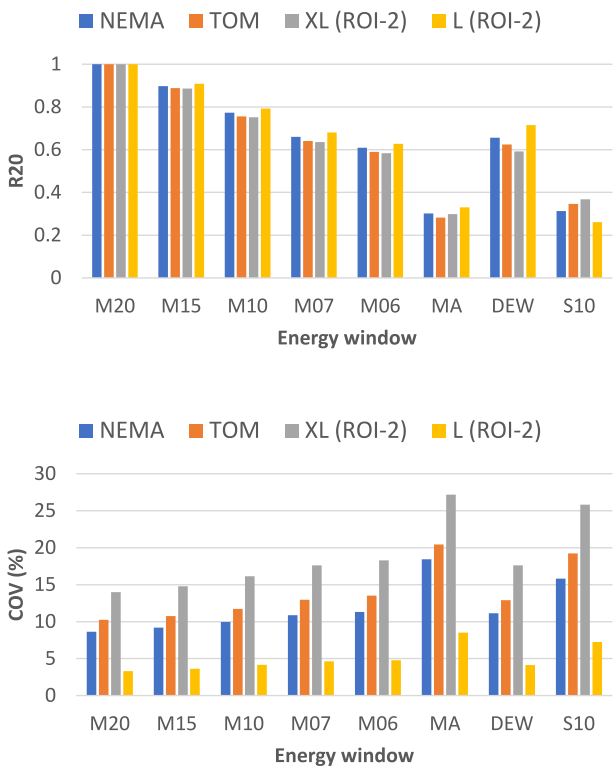

Fig. 3 Mean number of reconstructed counts per pixel relative to the 20% wide symmetric energy window (top) and COV in uniform parts of the four phantoms (bottom)

COV in the uniform part of the four phantoms for the six main energy windows, the secondary window, and when using manufacturer's DEW. In this figure, the results are given in L and XL for ROI – 2 whose borders are far away from the phantom walls in order to avoid any effect of the spatial resolution. The R20 values for the other ROIs in L and XL can be found in Additional file 1. The number of reconstructed counts systematically decreased when reducing the width of the symmetric window; for the narrowest windows, M06 and M07, the total number of reconstructed counts was only about 60–65% of the counts obtained with M20. A very similar reduction is observed when using DEW as implemented by the manufacturer. The reduction was more drastic for MA window with only about 30% of the counts obtained with M20. COV followed an inverse trend and increased when going from M20 to M06 and DEW. COV for DEW was very close to COV obtained with M07 and M06. MA was characterised by the largest COV with values about twice those observed with M20.

Decreasing the width of the photopeak-centred energy window from 20 down to 6% led to the following observations. In NEMA, RF (Fig. 4) increased in the air insert and decreased in the water and Teflon inserts, reaching a very low value in this hard insert for the narrowest windows. In TOM, RCcold (Fig. 5) and RChot (Fig. 6) increased. It was also observed that RF, RCcold and RChot had generally almost identical values for M06 and M07.

Using MA, RF was larger than with M06 in air but lower in water and Teflon (Fig. 4). RC of the largest (≥ 12 mm) cold rods (Fig. 5) and of all hot rods (Fig. 6) were equal or superior to the one obtained with any symmetric window.

With the manufacturer's DEW scatter correction, RF (Fig. 4) in water and Teflon inserts were the lowest and in the air insert ranked the second highest just below MA. RCcold were the highest for all but the smallest cold rods (Fig. 5) and largely the lowest for the hot rods (Fig. 6), reaching a null value when rod diameter was below 13 mm.

PostReconDEW RF (Fig. 4) was slightly positive in air but largely negative in water and Teflon inserts. PostReconDEW RCold (Fig. 5) and RChot (Fig. 6) were superior to their DEWimg counterparts in all but the thinnest rods.

The calibration factor depended slightly on the phantom and ROI used (Additionnal File 2). They generally were the highest for the smallest ROI, the lowest for ROI0 and were always almost identical for the three ROIs larger than the phantom physical size.

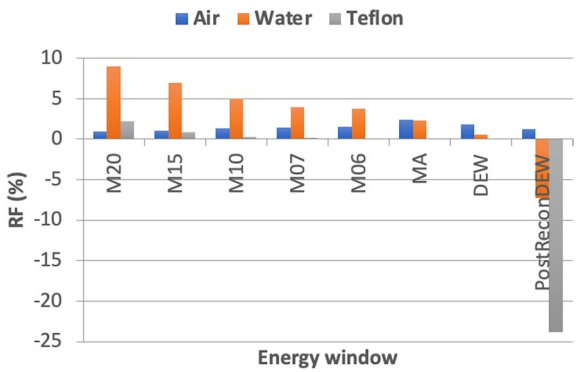

Fig. 4 Residual fraction in inserts of NEMA

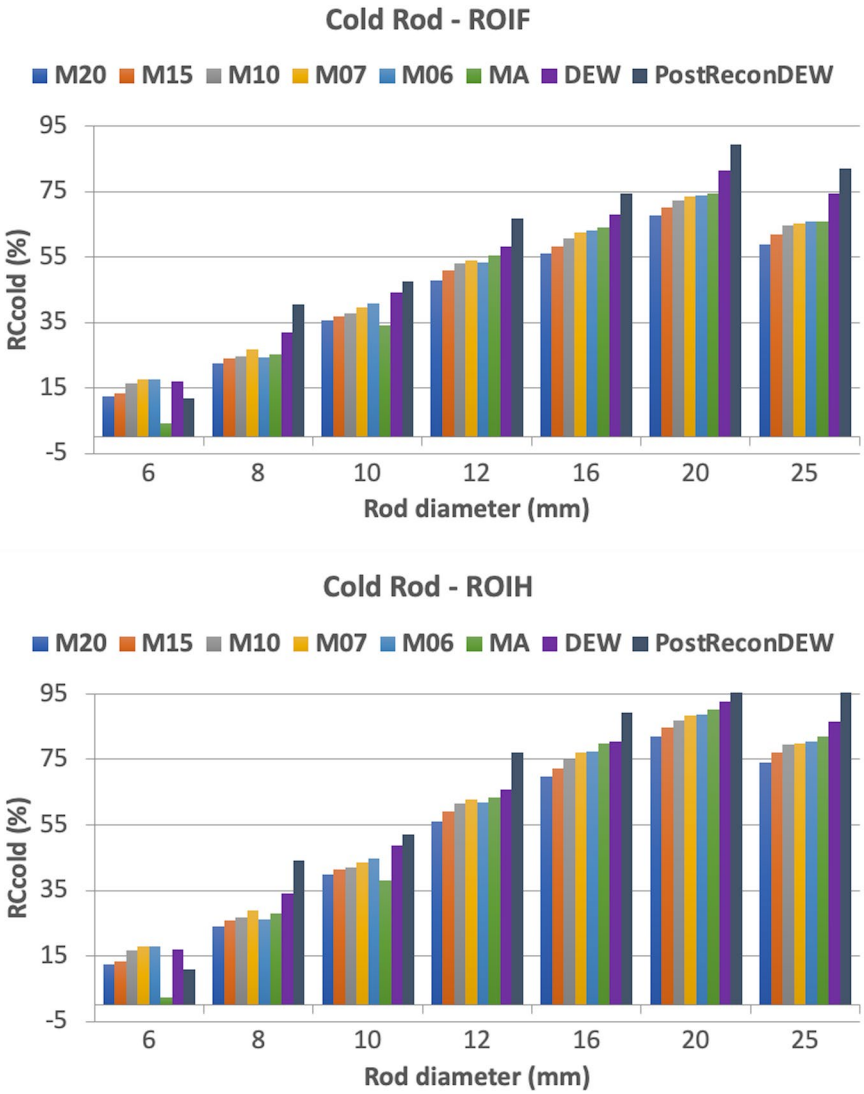

Fig. 5 Cold rod recovery coefficient in ROIF (top) and ROIH (bottom)

Finally, the quantification error (Fig. 7) in absolute value systematically decreased with the width of the symmetric energy window. It was the lowest with MA when L was used as calibration or activity measurement phantom, but almost as poor as with M20 for NEMA when using the calibration factor recorded with XL. The quantification accuracy (in absolute value) with manufacturer's DEW was comparable to the accuracy with M06 or MA depending on the phantom pair and the ROI size in the calibration phantom considered.

Discussion

For the recently introduced CZT detectors in SPECT, the use of similar width energy windows to those used with NaI scintillators is highly questionable with respect to the better energy resolution provided by these direct detectors [2–4, 18]. Likewise, a simple copy and paste of energy window-based SC techniques developed for the NaI

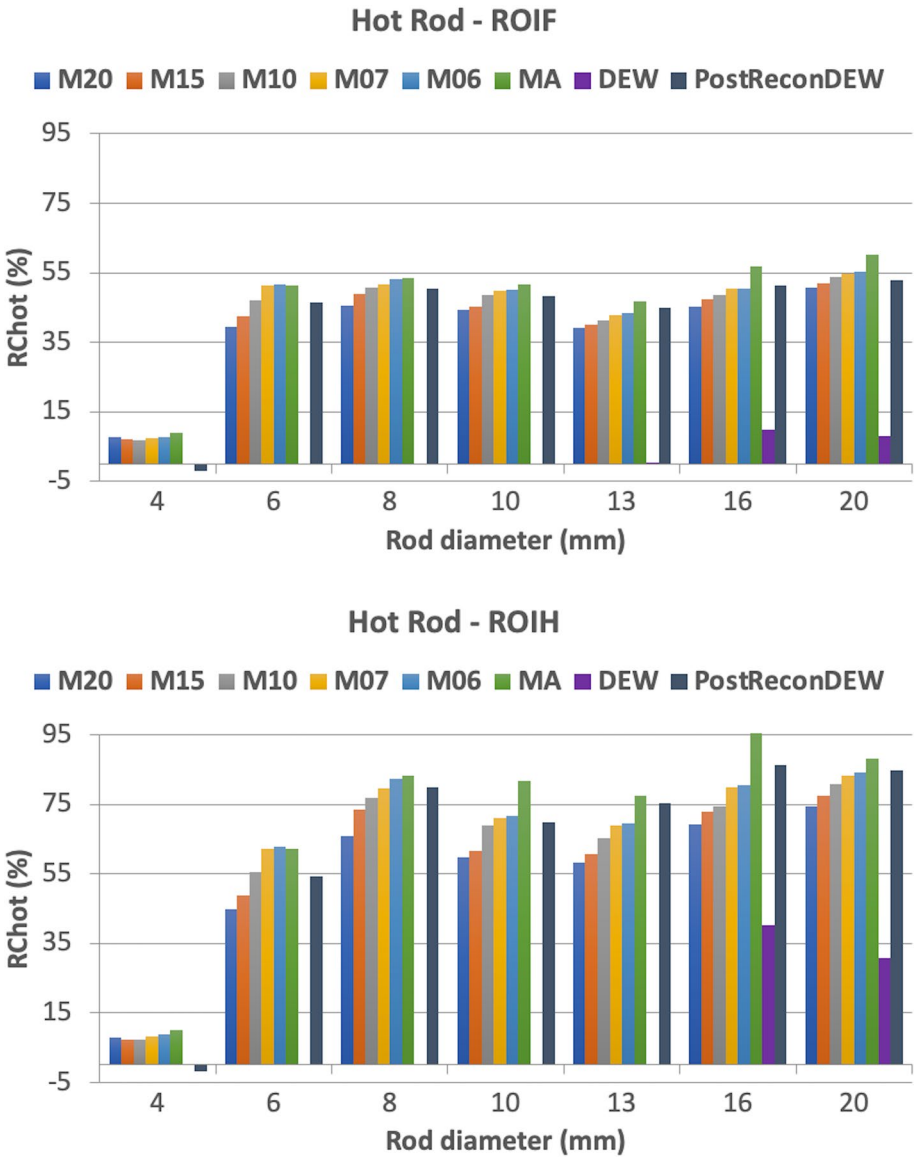

Fig. 6 Hot rod recovery coefficient in ROIF (top) and ROIH (bottom). RC is zero for the five smallest rods with DEW

detectors can be regarded with suspicion in light of the aforementioned better energy resolution but also the structurally different scatter spectra between the two types of detectors [2, 9].

As mentioned previously, SC as implemented by the manufacturers is not optimal and should be reconsidered [9, 19]. In our previous study [11], we observed lower recovery coefficients for hot rods in a cold background with SC than without SC when imaging with the new full ring or dual-head CZT SPECT systems. Moreover, with two of the three CZT systems compared, namely GE Healthcare Discovery and Starguide, the thinnest hot rods were surprisingly erased from the final images when the manufacturer's DEW was applied to correct for scatter.

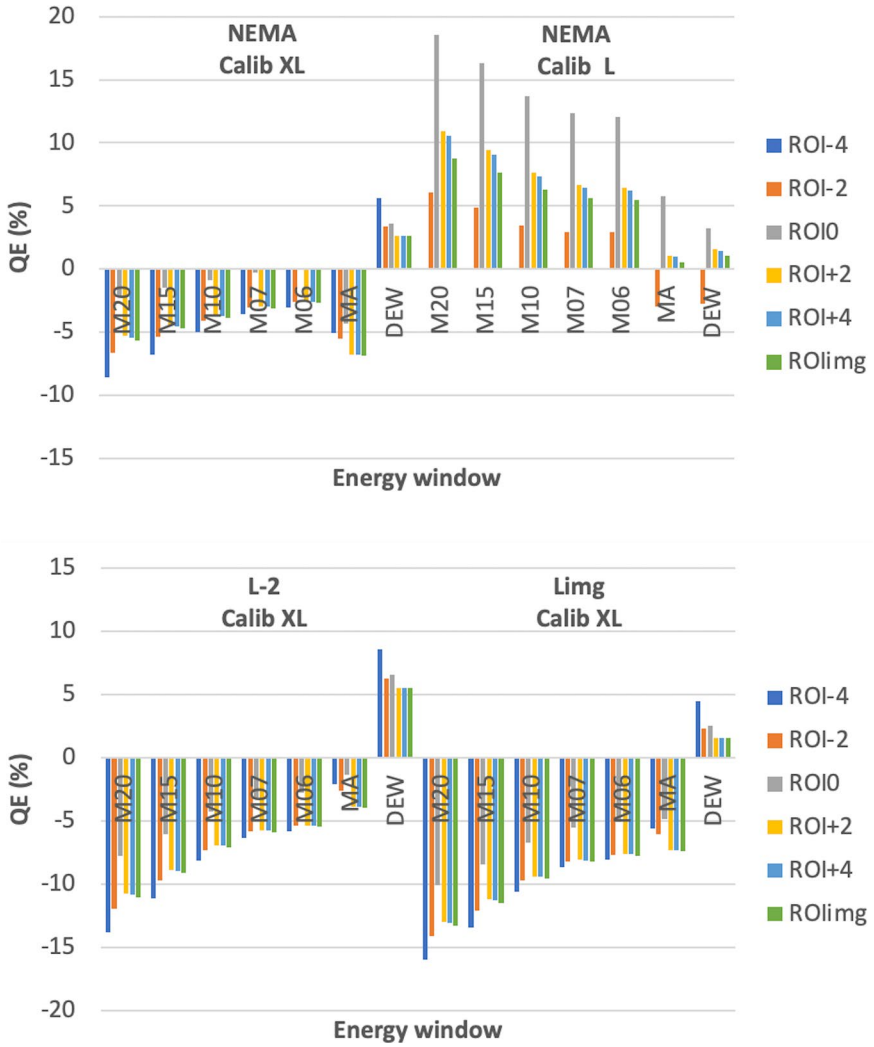

Fig. 7 Quantification error in NEMA (top) using XL or L as calibration phantom and in L (bottom) using XL as calibration phantom. The calibration factors were determined using six ROIs of different sizes with XL and five with L

The energy resolution at 140 keV of actual NaI detectors used in SPECT systems is about 9–10% full width at half-maximum, and energy windows of 15–20% width are usually adopted. As their energy resolution was measured to be 5–6% [4, 20, 21], simple reasoning would therefore lead to 8–10% width for the energy windows used with CZT detectors. A similar suggestion was already explored for a CZT dual head system [18]. A reduction of the energy width was the first approach of the present study. As the scatter spectrum of CZT is structurally different from NaI and with fewer scatter photons detected above the photopeak [2, 9], an asymmetric energy window starting at 140 keV and extending up to 154 keV was the second approach of this study. The third approach was to apply the standard DEW technique used by the manufacturer for SC, but post-reconstruction whereas the manufacturer's software performed the scatter correction in the iterative loop of the reconstruction. The manufacturer's default, at the time of this investigation, energy windows (M20 and S10) and k value (see above DEW equation)

were used. The residual fraction and recovery coefficients were computed using the DEW equation from the images reconstructed independently with attenuation correction and resolution recovery for M20 and S10 windows, and compared to their values obtained from the DEW images directly provided by the manufacturer's software. This last approach was inspired from the DEW SC implemented by the manufacturer of the competitor ring CZT SPECT system, namely Spectrum Dynamics Veriton, at the time of this study: the images obtained from the photopeak main window and the scatter window are separately reconstructed and subtracted using the above DEW equation [11].

As expected, the reduction of the width of the main energy window or using a fully asymmetric one resulted in a decrease in the number of reconstructed counts and a concomitant increase of the noise in the reconstructed images for these data, corresponding to an identical acquisition time (Fig. 3). The manufacturer's scatter correction with DEW resulted in images with reconstructed counts and noise levels similar to those obtained with M06 or M07. The DEW technique is widely accepted for clinical use, therefore the noise level recorded with M06 or M07 should not be an obstacle to their use for clinical applications.

In water and Teflon inserts of NEMA (Fig. 4), RF decreased with the main energy window width. A still lower RF was observed with MA and manufacturer's DEW related to the lowest RF. These observations complied with the photon energy loss during Compton interaction and the reduction of the energy window extension in the low energy part of the spectrum. In the air insert the trend was reversed, with the narrowest symmetric windows and MA showing the largest RF. DEW led to RF in air between those obtained with M06 and MA. An important decrease of RF in water and Teflon but an increase in air when using scatter correction was previously observed with NaI as well as CZT-based detectors [10, 11] for recordings made with the same NEMA NU2-1994 phantom.

In perfect agreement with RF behaviour observed in water and Teflon inserts of NEMA, RCcold (Fig. 5) of the largest ($\geq$12 mm) plastic rods of TOM increased when reducing the width of the symmetric window; this ranked the second highest with the asymmetric window and was the highest when performing the manufacturer's DEW scatter correction. Nevertheless, the differences between M06, M07 and MA were small and the noise could have overridden these differences, especially in the case of the thinnest rods ($\leq$10 mm) where the number of pixels in the ROI was small. An increase of RCcold with rod diameter was clearly evidenced (Fig. 5) with possible saturation above 16 mm. However, a difference in image texture has been reported between the phantom periphery and central parts with this CZT ring SPECT [3, 11] whose origin could not be defined. The SPECT resolution was also found to be about 1 mm larger at the centre of the field of view than the periphery [4]. The small RC decrease between the off-centre 20 mm rod and the central 25 mm rod could be related to these observations. The RCcold values observed for this ring CZT SPECT system with M20 and M15 or with DEW scatter correction were in the same range that RCcold obtained with NaI-based dual-head cameras or other CZT-based SPECT systems [10, 11].

RChot (Fig. 6) also increased when the width of the main symmetric window decreased. The highest RChot values were obtained with MA whereas they were the lowest, being equal to zero for most ($\leq$13 mm) of the hot rods, when images were scatter corrected with the manufacturer's DEW. This indicated a probable scatter

over-correction by DEW. RChot also seemed independent on rod size for diameters above 6–8 mm, a behaviour quite different from the NaI dual-head systems [10, 11]. Under the hypothesis of a classical partial volume effect on contrast recovery in hot cylindrical objects [22, 23], this would indicate a full width at half maximum resolution in the range 3–4 mm (6–8 mm divided by 2). This estimation is in good agreement with the 3.6–4.1 mm SPECT resolution recently measured in scatter medium for this system [4].

In summary, the reduction of the photopeak energy window width had the expected results of a lower residual fraction in water and Teflon inserts of the NEMA phantom, an enhanced contrast recovery in both cold and hot rods of the TOM phantom, a decrease in sensitivity coupled to an increase of the noise in the phantom uniform parts. The decrease of RF and RC were not linear and seemed to saturate at 6–7% window width. This would indicate that scatter rejection by a photopeak-centred energy window is maximal with a 6–7% window width.

The asymmetric energy window targets the part of the spectrum where detected photons are the least likely to have scattered [2, 9, 18]. With this window, RF were slightly lower and RC slightly higher or equal to the values obtained with the 6% symmetric energy window. This reinforced the above conclusion that a large part of the scattered photons was discarded with a 6–7% wide photopeak-centred window, and that this is the best result for scatter rejection that can be obtained with energy windowing for this CZT detector.

DEW as implemented by the manufacturer behaved very strangely in this system. The thinnest hot rods disappeared from the scatter corrected images and the recovery coefficients for the larger rods were very low, and much lower than without the scatter correction. Moreover, the 3D views of Fig. 2 shows that the largest hot rods seemed to be eroded from periphery to centre in radial direction and were no more uniform in axial direction. This strange behaviour could be, at least partially, linked to the presence of hot areas (cold rods and grid) on either side of the rods [11].

The PostReconDEW RF (Fig. 4) and RC (Figs. 5 and 6) differed notably from those obtained from the DEWimg. Largely negative RF values were obtained in water and Teflon (Fig. 4) showing a probable overestimation of scatter in these large cold rods. An overestimation of scatter in cold areas could also explain the highest RCcold observed for all but the thinnest cold rod when using DEW (Fig. 5). The PostReconDEW recovery coefficients in the hot rods (Fig. 6) reached values similar to those of M06img-M07img, again with the exception of the two thinnest rods. DEW is not a fully correct scatter correction technique. Moreover, the tailing should be taken into account [9] and this was not the case in the manufacturer's software version used in this study. PostReconDEW results shows nevertheless that the hot rods should be present in the DEWimg contrary to what was observed. We only have access to the manufacturer's software in standard user-mode, which precluded deeper analysis of the origin of the absence of most hot rods from the DEWimg.

Taken together, the results obtained with M06-M07, MA and PostReconDEW showed that a narrow 6–7% wide energy window could be used to efficiently reject scatter with this CZT detector when imaging with ^{99m}Tc, while obtaining a final noise level very similar to the one observed when using a wider energy window and the standard DEW

technique to correct for scatter. Moreover, the noise level could perhaps be reduced by the fusion of M06 and MA in a 136–154 keV (asymmetric 12%) window, as scattered photons are almost absent from the CZT spectrum above 140 keV [2, 18].

Narrow windows will still contain scattered photons and an additional SC technique would remain necessary even with a single peak emitter like ^{99m}Tc. However, thanks to a reduced scatter fraction in these windows compared to the conventional wider windows, the accuracy of the scatter correction technique would be less crucial. Therefore, the energy window-based scatter correction techniques [24], among them DEW or TEW, should not necessarily be discarded for CZT detectors. However, they need to be adapted and retuned according to the properties of CZT [9] that differ from NaI, for which these techniques were developed and validated. Such an adaptation has been for example proposed and shown successful for a cardiac dedicated CZT-based system [9]. Monte Carlo simulations would certainly also be very helpful, and efforts to develop Monte Carlo simulations of CZT SPECT systems [25] should be encouraged and supported.

Likely due to ease of implementation, until now SC in clinical SPECT was mainly performed using energy window-based techniques [24]. Now, SPECT is most often one component of a hybrid SPECT-CT system. Therefore, SC using CT data and the related tissue information should be considered as a viable alternative to energy window-based SC [24]. Effective scatter source estimation (ESSE) was, for example, used successfully by one manufacturer [10, 24] for a NaI-based SPECT-CT system. The scatter point kernels used in ESSE should be redefined because of the specific characteristics of the CZT scatter spectrum. Analytical photon distribution interpolated (APDI) also uses tissue density. APDI was compared to TEW for SC in ^{177}Lu imaging with NaI SPECT, and was found to perform better in soft tissues [19].

In the course of this study, we were informed that a revised DEW implementation was under study for this ring CZT SPECT system by the manufacturer. For this, narrower main and secondary windows will be used and the correction will remain applied during the reconstruction in the iterative loop. We shared our list-mode files with the manufacturer and were informed that this new DEW implementation led to results approaching those obtained in this study with the narrowest windows and that all hot rods were present in the scatter corrected images. During the review process of this manuscript, we learned that the manufacturer had started the release of this new DEW implementation and we hope to have in the next future the opportunity to reconstruct our data with this modified software.

While this study was conducted with one particular ring CZT SPECT-CT, it is highly likely that its general conclusion on the use of a narrow main energy window could be extended to other CZT SPECT systems available on the market. This study focused on ^{99m}Tc, but multi-peak emitters such as ^{123}I, ^{111}In, ^{177}Lu, to name a few, should be the subject of additional studies. Indeed, the down-scatter from the higher energy peaks contaminates the low energy windows [24]. Therefore, the narrowing of the energy window cannot successfully reject all the down-scattered photons, and an additional scatter correction strategy remains necessary. This study used OSEM without any noise reduction techniques. This was possible thanks to the high number of recorded counts. Before its transposition in clinics, complementary works on the use of a noise reduction technique

would most probably be needed. This was however considered out of the scope of this methodology-oriented work. One of the reasons is that the technique parameters should generally be specifically tuned for each exploration type.

Conclusions

A narrow symmetric or a fully asymmetric energy window was shown to discard scattered ^{99m}Tc photons from final reconstructed images in a way that was at least as efficient as the standard dual energy window with two wide energy windows recommended by the manufacturer of the ring CZT SPECT system at the time of this investigation. In particular, this window strategy avoided the absence of the smallest hot objects observed in images produced with the dual energy window scatter correction. These conclusions are very likely to also apply to other CZT SPECT systems present on the market today, but should not be directly extended to other isotopes, especially the multi-peak emitters.

Abbreviations

Ames	Measured activity concentration
APDI	Analytical photon distribution interpolated
Atrue	True activity concentration
CF	Conversion factors
COV	Coefficient of variation in percent
CT	X-ray computed tomography
CZT	Cadmium zinc telluride
DEW	Dual energy window
ESSE	Effective scatter source estimation
L	Uniform cylindrical phantom of medium size
M20img_MNC	Mean number of counts in M20img
MA	140–154 KeV asymmetric main energy window
MAimg	Image reconstructed from the MA projections with attenuation correction and resolution recovery
MNC	Mean number of counts
M06	Photopeak-centred main energy window with 6% full width
M07	Photopeak-centred main energy window with 7% full width
M10	Photopeak-centred main energy window with 10% full width
M15	Photopeak-centred main energy window with 15% full width
M20	Photopeak-centred main energy window with 20% full width
M06img	Image reconstructed from the M06 projections with attenuation correction and resolution recovery
M07img	Image reconstructed from the M07 projections with attenuation correction and resolution recovery
M10img	Image reconstructed from the M10 projections with attenuation correction and resolution recovery
M15img	Image reconstructed from the M15 projections with attenuation correction and resolution recovery
M20img	Image reconstructed from the M20 projections with attenuation correction and resolution recovery
NaI	Sodium iodide
NEMA	NU2-1994 attenuation and scatter correction accuracy phantom
OSEM	Ordered subset expectation maximisation
PostReconDEW	DEW scatter corrected data obtained from the reconstructed images of M20 and S10 windows.
QE	Percent quantification error
RC	Recovery coefficient
RCcold	Recovery coefficient in a cold rod
RChot	Recovery coefficient in a hot rod
RF	Residual fraction
ROI	Region of interest
ROIF	Region of interest of full rod physical diameter
ROIimg	Region of interest encompassing the whole reconstructed image
ROIH	Region of interest of half rod physical diameter
ROI0	Cylindrical region of interest with a diameter and a height equal to the physical diameter and height of the phantom
ROI-n	Cylindrical region of interest with a diameter and a height n cm smaller than the physical diameter and height of the phantom
ROI + n	Cylindrical region of interest with a diameter and a height n cm larger than the physical diameter and height of the phantom
RR	Resolution recovery
S10	114–126 KeV (10%) secondary energy window
S10img	Image reconstructed from the S10 projections with attenuation correction and resolution recovery
S10img_MNC	Mean number of counts in S10img

SC	Scatter correction
SC_MNC	Scatter corrected mean number of counts
SPECT	Single-photon emission computed tomography
TEW	Triple energy window
TOM	Custom contrast phantom
XL	Uniform cylindrical phantom of large size

Supplementary Information

The online version contains supplementary material available at https://doi.org/10.1186/s40658-025-00793-w.

Supplementary file 1 (PDF 235 KB)

Acknowledgements
The authors would like to thank Med Dr Gaetan Letesson, head of the nuclear medicine department of CHR Citadelle Liège, for providing access to the ring CZT SPECT system used in this work. The help of Dr Martina Stella (GE Healthcare Benelux) and Mr Vincent Bartholomé (GE Healthcare Benelux) during data acquisition and for the rebinning of list mode files is gratefully acknowledged. We are grateful to the reviewers whose detailed and critical reading and very constructive remarks have undoubtedly led to improvements of this report.

Author contributions
AS designed the experiments, participated in data acquisition, analysed the images and drafted the manuscript. CB performed all acquisitions, participated in the image analysis and manuscript writing. Both authors read and approved the final manuscript.

Funding
Not applicable.

Availability of data and materials
The datasets used and/or analysed during the current study are available from the corresponding author on reasonable request.

Declarations

Ethics approval and consent to participate
Not applicable.

Consent for publication
Not applicable.

Competing interests
The authors declare that they have no competing interests.

Received: 25 February 2025 Accepted: 11 August 2025
Published online: 20 August 2025

References

1. Desmonts C, Bouthiba MA, Enilorac B, Nganoa C, Agostini D, Aide N. Evaluation of a new multipurpose whole-body CZT-based camera: comparison with a dual-head Anger camera and first clinical images. EJNMMI Phys. 2020;7:18. https://doi.org/10.1186/s40658-020-0284-5.
2. Ito T, Matsusaka Y, Onoguchi M, Ichikawa H, Okuda K, Shibutani T, et al. Experimental evaluation of the GE NM/CT 870 CZT clinical SPECT system equipped with WEHR and MEHRS collimator. J Appl Clin Med Phys. 2021;22:165–77. https://doi.org/10.1002/acm2.13158.
3. Hoog C, Koulibaly P-M, Sas N, Imbert L, Le Rouzic G, Popoff R, et al. 360° CZT-SPECT/CT cameras: ^{99m}Tc- and ^{177}Lu-phantom-based evaluation under clinical conditions. EJNMMI Phys. 2024;11:89. https://doi.org/10.1186/s40658-024-00684-6.
4. Zorz A, Rossato MA, Turco P, Colombo Gomez LM, Bettinelli A, De Monte F, et al. Performance evaluation of the 3D-ring cadmium-zinc-telluride (CZT) starguide system according to the NEMA NU 1–2018 standard. EJNMMI Phys. 2024;11:69. https://doi.org/10.1186/s40658-024-00671-x.
5. Vergnaud L, Badel J-N, Giraudet A-L, Kryza D, Mognetti T, Baudier T, et al. Performance study of a 360° CZT camera for monitoring ^{177}Lu-PSMA treatment. EJNMMI Phys. 2023;10:58. https://doi.org/10.1186/s40658-023-00576-1.
6. Jaszczak RJ, Floyd CE, Coleman RE. Scatter compensation techniques for SPECT. IEEE Trans Nucl Sci. 1985;32:786–93.
7. Ogawa K, Harata Y, Ichihara T, Kubo A, Hashimoto S. A practical method for position-dependent Compton scatter compensation in single photon emission CT. IEEE Trans Med Imaging. 1991;10:408–12.
8. Ichihara T, Ogawa K, Motomura N, Kubo A, Hashimoto S. Compton scatter compensation using the triple-energy window method for single- and dual-isotope SPECT. J Nucl Med. 1993;34:2216–21.

9. Pourmoghaddas A, Vanderwerf K, Ruddy TD, Wells RG. Scatter correction improves concordance in SPECT MPI with a dedicated cardiac SPECT solid-state camera. J Nucl Cardiol. 2015;22:334–43. https://doi.org/10.1007/s12350-014-0008-0.
10. Seret A, Nguyen D, Bernard C. Quantitative capabilities of four state-of-the-art SPECT-CT cameras. EJNMMI Res. 2012;2:45. https://doi.org/10.1186/2191-219X-2-45.
11. Seret A, Bernard C. Quantitative capabilities of commercial CZT SPECT-CT cameras. EJNMMIPhys. 2025;12:44. https://doi.org/10.1186/s40658-025-00754-3.
12. National Electrical Manufacturers Association (NEMA). Performance measurements of positron emission tomographs, NEMA standards publication NU2. Washington, DC: NEMA; 1994.
13. Saldarriaga Vargas C, Rodríguez Pérez S, Baete K, Pommé S, Paepen J, Van Ammel R, et al. Intercomparison of ^{99m}Tc, ^{18}F and ^{111}In activity measurements with radionuclide calibrators in Belgian hospitals. Phys Med. 2018;45:134–42. https://doi.org/10.1016/j.ejmp.2017.12.011.
14. Graham R, Morland D, Cade S, Imbert L, Panagiotidis E, Kurth J, et al. EANM position paper on challenges and opportunities of full-ring 360° CZT bone imaging: it's time to let go of planar whole-body bone imaging. Eur J Nucl Med Mol Imaging. 2025;52:1200–9. https://doi.org/10.1007/s00259-024-06906-4.
15. Carnegie-Peak L, Taprogge J, Murray I, Flux GD, Gea J. Quantification and dosimetry of small volumes including associated uncertainty estimation. EJNMMI Phys. 2022;9:86. https://doi.org/10.1186/s40658-022-00512-9.
16. Danieli R, Stella M, Leube J, Tran-Gia J, Marin C, Uribe CF, et al. Quantitative ^{177}Lu SPECT/CT imaging for personalized dosimetry using a ring-shaped CZT-based camera. EJNMMI Phys. 2023;10:64. https://doi.org/10.1186/s40658-023-00586-z.
17. Zeintl J, Vija HA, Yahil A, Hornegger J, Kuwert T. Quantitative accuracy of clinical ^{99m}Tc SPECT/CT using ordered-subset expectation maximization with 3-dimensional resolution recovery, attenuation, and scatter correction. J Nuc Med. 2010;51:921–8. https://doi.org/10.2967/jnumed.109.071571.
18. Arvola S, Seppänen S, Timonen KL, Rautio P, Ettala O, Anttinen M, et al. Detection of prostate cancer bone metastases with fast whole-body ^{99m}Tc-HMDP SPECT/CT using a general-purpose CZT system. EJNMMI Phys. 2022;9:85. https://doi.org/10.1186/s40658-022-00517-4.
19. Uribe CF, Esquinas PL, Tanguay J, Gonzalez M, Gaudin E, Beauregard J-M, et al. Accuracy of ^{177}Lu activity quantification in SPECT imaging: a phantom study. EJNMMI Phys. 2017;4:2. https://doi.org/10.1186/s40658-016-0170-3.
20. Le Rouzic G, Zananiri R. First performance measurements of a new multi-detector CZT-based SPECT/CT system: GE StarGuide. J Nuc Med. 2021;62(S1):1125.
21. Ferri V, Zananiri R, Iagaru A. Performance evaluation of a novel multi-detector CZT-based SPECT/CT system using Tc99m and Lu177. J Nucl Med. 2022;63(S1):2440.
22. Rousset O, Zaidi H. Correction for partial volume effects in emission tomography. In: Zaidi H, editor. Quantitative analysis in nuclear medicine imaging. 1st ed. New York: Springer Inc; 2006.
23. Cherry SR, Sorenson JA, Phelps ME. Physics in nuclear medicine. 4th ed. Philadelphia: Elsevier Inc.; 2012.
24. Hutton BF, Buvat I, Beekman FJ. Review and current status of SPECT scatter correction. Phys Med Biol. 2011;56:R85-112. https://doi.org/10.1088/0031-9155/56/14/R01.
25. Pretorius PH, Liu C, Fan P, Peterson M, Ljunberg M. Monte Carlo simulations of the GE Discovery Alcyone CZT SPECT systems. IEEE Trans Nucl Sci. 2015;62:832–9. https://doi.org/10.1109/TNS.2015.2433533.

Publisher's Note